13th ewtec 2019 Proceedings of the 13th European Wave and Tidal Energy Conference 1-6 Sept 2019, Naples, Italy

Numerical Benchmarking of selected Efficiency-Aware Reactive Control Strategies on the InfinityWEC Wave Energy Converter

Ahmed Rashid, Mikael Sidenmark

Abstract—**Reactive control has been shown to be the optimal control strategy for a point absorbing wave energy converter (WEC), in terms of achieving the highest power capture. However, in the simplest form, such control sets the WEC in a resonant state with the wave frequency, which requires reciprocating power flows with very high peak power, large force, high velocity and long stroke length to be provided by the power take-off (PTO). This makes it difficult to find a practical, efficient and economically viable solution to provide this type of control.**

The main objective of this paper is to present a time-efficient numerical simulation model and performance analysis of the novel InfinityWEC, developed by Ocean Harvesting Technologies AB. The PTO of the WEC comprises of a ballscrew actuator system and a flywheel-based Kinetic Energy Recovery System (KERS) with capabilities to provide advanced reactive control, which introduces PTO losses and constraints for maximum velocity, force and stroke length in its design to mitigate the mentioned drawbacks of conventional reactive control.

In order to make the simulation model time efficient, the hull geometry of the InfinityWEC has first of all been simplified to a cylinder with the same width, mass and volume of the actual hull. A nonlinear model of the cylinder in heave mode, which is the most important degree of freedom (DoF) for a point absorbing device, is then derived and implemented. The performance of the system is finally analyzed by comparing three different efficiency-aware reactive control strategies with the objective of maximizing export power while considering constraints for maximum allowed PTO force, velocity, stroke length and limited hull volume.

The control strategies, analyzed in this report, are linear reactive control (LRC), "polynomial" reactive control (PRC) and nonlinear model predictive control (NMPC). LRC and PRC are passive control techniques, whose coefficients are optimally-tuned for each sea state using an optimization algorithm. LRC is studied extensively in the wave power literature and serves as the reference case in the study. PRC is novel to authors knowledge and can be considered as a higher-order extension that gives extra degree of flexibility to LRC with the objective to improve performance and constraint-handling capability. NMPC is an active control strategy, which optimizes the PTO force and buoy motion at each time instant by knowing the incoming wave a few seconds in advance.

Annual simulations are run with the three control strategies in a selected sea site and results are analyzed in terms of performance, load case and constraint-handling capability.

Index Terms—**wave power, power take-off, flywheel storage, kinetic energy recovery system, efficiency-aware control, nonlinear model predictive control, polynomial control, reactive control, InfinityWEC**

I. Introduction

WAVE power represents an enormous exploitable energy resource estimated to 29,500 TWh/yr, [1], which is close to 50% more than the current global electricity generation. Wave energy devices has been studied extensively since the 70's and a large number of concepts have been proposed and tested. However, due to the multidisciplinary complex nature of developing an economically viable solution to harvest

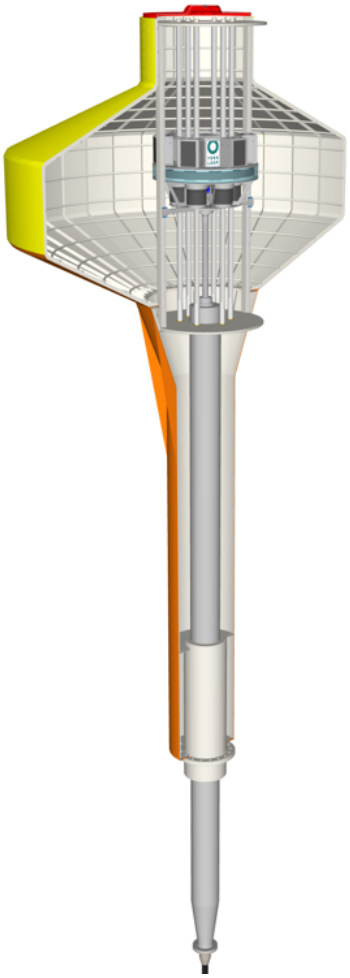

Fig. 1. InfinityWEC wave energy converter.

Paper ID number:1586- Conference track: GPC

Submitted for the Proceedings of the 13th European Wave and Tidal Energy Conference, EWTEC, 2019. This study is part of a larger project with topic "Model Validation with Numerical Wave Tank and LCoE-Based Design Optimization of the InfnityWEC Wave Energy Converter", that is funded by Swedish Energy Agency.

F. A. Rashid, Ocean Harvesting Technologies AB, Campus Gräsvik 28, 37175 Karlsrkona, Sweden (e-mail: ahmed.rashid@oceanharvesting.com).

S. M. Sidenmark, Ocean Harvesting Technologies AB, Campus Gräsvik 28, 37175 Karlsrkona, Sweden (e-mail: mikael.sidenmark@oceanharvesting.com).

this resource, the potential of wave energy remains untapped. The main reason for the lack of exploitation of the wave energy resource is due to the random and highly variable motion of ocean waves, which imposes the following challenges: 1) fatigue and wear due to the extremely high number of load cycles, 2) input power with high peak-to-average ratio to the PTO, 3) high peak force, velocity and stroke length in the PTO, 4) survival in extreme weather without violating the constraints of the PTO. This in turn implies oversizing of machine components with sufficient safety design factors to withstand the fatigue from continuous cyclic motion over the design life time of the device, to manage the peaks in the input power, to provide the required peak PTO force, velocity and stroke length, and to survive in extreme weather conditions. The high peak-to-average power and high PTO force cause high capital expenditure of the system, low utilization of components and poor quality with high intermittency of the generated electricity. In order to decrease the cost and increase the utilization of the system of electrical infrastructure, and also to meet grid quality requirements, it is crucial that the power is smoothed efficiently with some form of energy storage before power is exported from the WEC. It is furthermore essential that the energy storage is integrated in the power take-off system in a way that does not compromise the power capture performance of the wave energy converter, i.e. without preventing force control capability of the device.

InfinityWEC wave energy converter, depicted in Fig. 1, is a novel system that has been designed to meet the outlined challenges, to provide an economically viable wave energy converter. The PTO system of the InfinityWEC uses ballscrew actuators and a flywheel-based Kinetic Energy Recovery System (KERS), which provides the necessary capability to provide advanced reactive force control as well as smoothing of the captured power to a nearly constant power output. The system is furthermore very light and efficient relative to the combination of high cycles, force, power, velocity and stroke length, it is designed for.

II. Background

OHT was founded in 2007 in Karlskrona to develop wave power technology. R&D has been focused on energy storage integration in the power take-off to smooth captured power and to improve the power capture performance. OHT's wave energy technology development has evolved through different technological approaches over the last 10 years. The initial WEC concept with winch actuator and on-board gravity-based storage for power-smoothing from each WEC (Fig. 2a) has been developed over the years to a system with hydraulic collection of power and central gravity-based storage to provide array level power smoothing and grid frequency regulation (Fig. 2b).

In 2017, OHT saw the recent development in electric vehicles, electric motors and power electronics and realized the opportunity of using the KERS (Kinetic Energy Recovery System) technology from the automotive industry to provide smooth controllable output

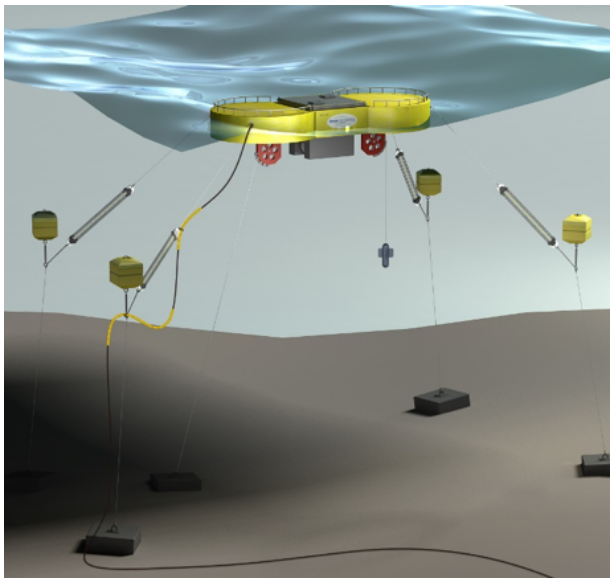

(a) Initial WEC concept with winch actuator and on-board gravity storage (2008-2012)

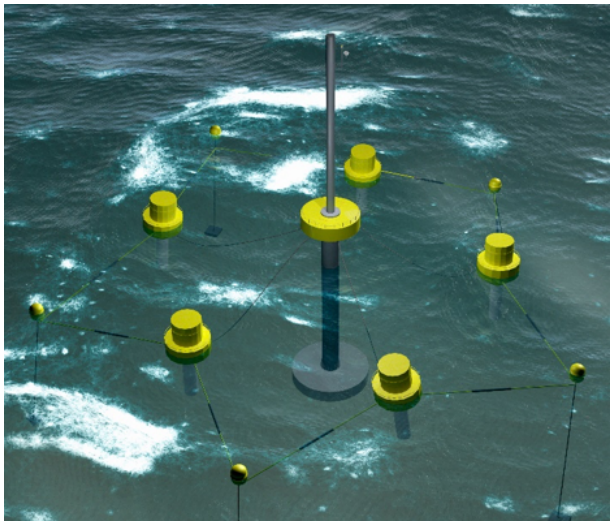

(b) System with hydraulic collection of power and central gravity storage (2013-2016)

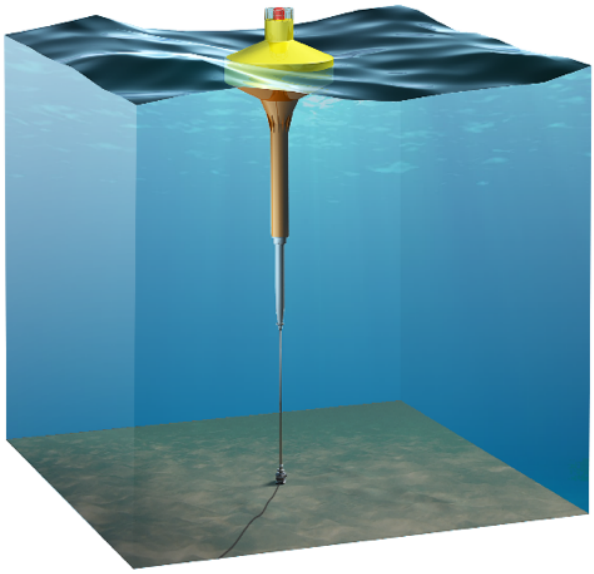

(c) InfinityWEC wave energy converter with ballscrew actuator and on-board flywheel storage (2017-)

Fig. 2. Wave energy solutions, developed by OHT over the years.

power and PTO force control. This led to the development of the InfinityWEC technology (Fig. 2c).

The InfinityWEC utilizes a novel direct-drive mechanical PTO technology that comprises of a modular ballscrew actuation system, frameless torque generators, a lead screw level adjustment system, and a novel hubless outer-ring flywheel unit, developed by Teraloop. The PTO is held in a fixed vertical position by the mooring system while the non-rotating ballscrews are pushed up and down through the PTO platform when the buoy is set in motion by the waves. The lead screw connects the PTO platform to the mooring system and is used to adjust the height of the PTO for tidal variations and to submerge the WEC to secure survival in storm conditions. A riser pipe from the oil & gas sector is used as mooring tether, an arrangement which provides a protected route for the power and communication cables inside the pipe and minimizes the bending of these cables, an issue with suspending dynamic cables from the hull in other WECs.

The ball nuts are integrated to the so-called frameless torque motors that are characterized with extremely high-torque density, as the name implies. The stators of the electric motors are connected electrically to the flywheel energy storage and to the export cables. The power flow through the system is managed by the power inverters. The number of drive units, comprising of a ballscrew, a generator and an power inverter, can be configured depending on the load requirements of the device. Fig. 3 shows a schematic of the electric KERS technology with four drive units, embodied in the InfinityWEC.

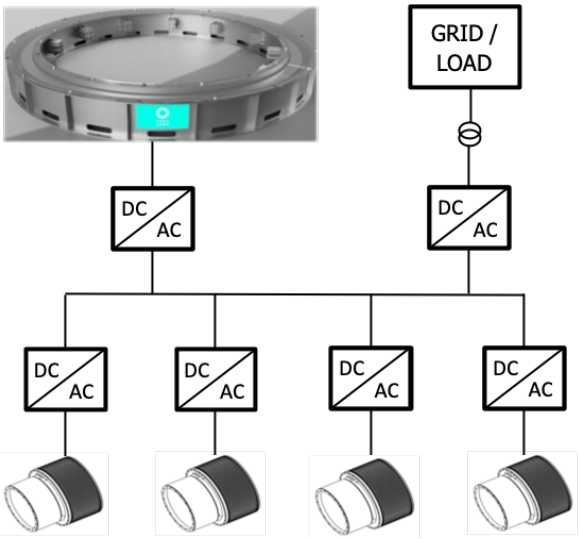

Fig. 3. Schematics of electrical KERS system with four drive units, comprising of integrated ballscrew-motor and frequency inverter

The working principle of the KERS technology, utilized by the InfinityWEC PTO is straightforward. Similar to an electric motor is used to brake a vehicle, generating and storing energy in the car battery for later use, the PTO of the InfinityWEC uses a flywheel storage system to store excessive energy to deliver both smooth controllable output power and the necessary reverse power for reactive control and pretension. In this way, KERS enables a full flexibility for the control system to optimize and apply reactive PTO force with the main objectives to: (i) maximize output power considering losses, (ii) limit buoy motion and prevent hard end-stops, (iii) limit PTO force, stroke-length, velocity and power to optimized design values to reduce cost. This type of control can be provided without prediction of wave input, but knowing the incoming wave motion a few seconds in advance makes it possible for the control system to better optimize the PTO force to achieve the control objectives with higher precision and higher annual output.

The design requirements for energy storage in the InfinityWEC are extremely demanding and the flywheel storage solution, offered by Teraloop, is identified to be the only technology that can meet them thanks to its unique design. Teraloop comprises of a thin outer ring flywheel rotor with permanent magnets integrated with the motor/generator rotor, which is located around the ballscrew assembly in InfinityWEC. The rotor is fully levitated by a magnetic levitation system using a combination of passive permanent magnet levitation and active electromagnetic stabilization. This hub-less rotor design without mechanical bearings eliminates both wear and fatigue issues and provides virtually unlimited cycle life time. The wide diameter enables high power rating and large storage capacity per unit mass of the device. The size of Teraloop's flywheel can effectively be increased to provide enough storage capacity to participate in the ancillary services market, thus, providing a possibility to increase revenues from the WECs.

III. System description

A. Buoy and power take-off

In order to make the simulation model time efficient, the hull geometry of the InfinityWEC has first of all been simplified to a cylinder with the same width, mass and volume. The hydrodynamic behaviour of the real geometry is expected to be very similar to a cylinder since the waterline will oscillate mainly at the widest part of the real hull. A cylindrical buoy has also been studied extensively in the wave power literature [2], thus, allowing the obtained results from this study to be related to previous works.

The physical and geometric parameters of the cylindrical buoy are summarized in Table I.

TABLE I
PHYSICAL AND GEOMETRICAL PROPERTIES OF THE STUDIED CYLINDRICAL BUOY

Symbol	Quantity	Value	Unit
d_b	Buoy diameter	15.0	m
h_b	Buoy height	2.55	m
A_{wp}	Water-plane area	176.7	m^2
V_b	Buoy volume	450.0	m^3
m_b	Buoy mass	74.0	ton

In this study, a detailed dynamic model of the machinery inside the buoy is omitted. However, the

losses in the power take-off are accounted by using the nominal efficiency values of the main drivetrain components of the InfinityWEC wave energy converter, which are summarized in Table II. These efficiency values are obtained from the suppliers of each component. In general, the efficiency of electric motors and inverters are not constant and will reduce mainly at low speed. To model losses more accurately, loss maps, expressing the efficiency of each component as a function of e.g. speed/voltage and torque/current needs to be included in the simulation. This data was not available on all components at the time of the study, which is why the simpler approach has been used. It can be expected that losses will be slightly higher when the efficiency of all electric components are modelled dynamically with loss maps. On the other hand, Coulomb friction has the highest contribution to the overall losses in mechanical actuators, thus, utilizing a constant efficiency model for the ballscrew leads to a sufficiently accurate approximation of the mechanical losses of the actuator.

TABLE II
EFFICIENCY OF DRIVETRAIN COMPONENTS

Component	Efficiency
Ballscrew Mechanical	95%
Ballscrew Generator	96%
Ballscrew Inverter	98%
Flywheel Inverter	98%
Flywheel Motor	96%
Output Inverter	98%

In this study, the physical constraints of the power take-off, such as maximum stroke length, tether force and velocity, and physical constraints of the hull, such as volume or height, are also considered. Their values are chosen according to the constraints of the InfinityWEC device and are summarized in table III.

TABLE III
SYSTEM CONSTRAINTS

Symbol	Quantity	Value	Unit
l_s^{max}	Max stroke length	5.0	m
F_t^{max}	Max tether force	3.0	MN
v_b^{max}	Max buoy velocity	2.0	m/s
h_b^{max}	Max buoy height	2.55	m

B. Environmental conditions

The Yeu island located in France is chosen to be the site of this study since it has been extensively used as a benchmark site in the wave energy literature ([2]–[4]). The sea bottom at the site location is assumed to be flat with constant water depth of 50 meters. The waves are assumed to be unidirectional. The wave scatter diagram of the site is shown in Fig. 4. The wave resource at Yeu is 25.5 kW/m wave front annually, which is considered to be a relatively mild wave resource. It should be noted that the InfinityWEC is designed for stronger wave climate with higher annual output.

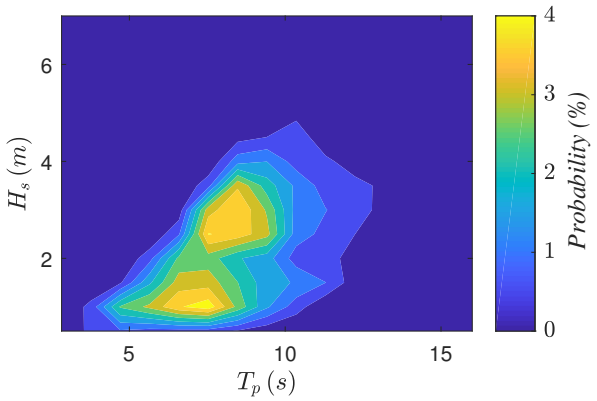

Fig. 4. Wave scatter in Yeu island site, France, [3].

IV. HYDRODYNAMIC MODEL

This section presents the hydrodynamic model of a generic wave energy converter. The derivation starts with a 6 DoF model, which is later reduced to 1 DoF model in heave to enable numerically-efficient simulation of the system. The hydrodynamic model in heave is further linearized for controller synthesis.

C. 6 DoF model

The force balance on a floating wave energy converter can be formulated as

$$\mathbf{M}\ddot{\mathbf{x}}(t) = \mathbf{F_e} + \mathbf{F_r} + \mathbf{F_{hs}} + \mathbf{F_{dr}} + \mathbf{F_g} + \mathbf{F_{pto}} \quad (1)$$

where $\mathbf{x}(t) = \begin{bmatrix} x(t) & y(t) & z(t) & \theta_x(t) & \theta_y(t) & \theta_z(t) \end{bmatrix}^T \in \mathbb{R}^{6\times 1}$, is the state vector with entries respective translational displacement in surge, sway and heave and rotational displacement in roll, pitch and yaw, $\mathbf{M} \in \mathbb{R}^{6\times 6}$ is the mass matrix, $\mathbf{F_e} \in \mathbb{R}^{6\times 1}$ is the wave excitation force, $\mathbf{F_r} \in \mathbb{R}^{6\times 1}$ is the radiation force, $\mathbf{F_{dr}} \in \mathbb{R}^{6\times 1}$ is the drag force, $\mathbf{F_{hs}} \in \mathbb{R}^{6\times 1}$ is the hydrostatic force, $\mathbf{F_g} \in \mathbb{R}^{6\times 1}$ is the gravity force, and $\mathbf{F_{pto}} \in \mathbb{R}^{6\times 1}$ is the machinery force from the power take-off. It should be noted that the time-dependence of all force terms in (1) is not explicitly shown. This is a convention, that is used throughout the report, to improve readability of equations.

The irregular excitation force can be pre-calculated based on hydrodynamic parameters and wave elevation prior to a numerical simulation. The wave elevation of an irregular wave can be represented as a linear superposition of N regular wave components with different amplitude, frequency and phase, i.e.

$$\eta(x,t) = \sum_{i=1}^{N} a_i cos(\omega_i t - k_i \xi(x,y) + \phi_i) \quad (2)$$

where t is time, $\xi(x,y)$ position along the wave's direction of travel, ϕ_i are random phases uniformly distributed between 0 and 2π, ω_i are angular frequencies, k_i are wavenumbers and a_i are random amplitudes,

which are taken to be Rayleigh distributed with mean square value

$$E[a_i^2] = 2S(\omega)\Delta\omega_i \tag{3}$$

where $S(\omega)$ is the wave spectrum and $\Delta\omega_i$ is the frequency step between two frequency components. The amplitudes can be approximately computed as

$$a_i \approx \sqrt{2S(\omega)\Delta\omega_i} \tag{4}$$

The wave spectrum is usually represented by different empirical expressions as a function of the significant wave height, H_s, and peak wave period, T_p.

Let us denote each wave component as η_i and say that each wave component is the real part of the complex-valued signal η_{ci}, i.e.

$$\eta_i = \Re\left[\eta_{ci}\right] = \Re\left[a_i e^{\omega_i t - k_i \xi(x,y) + \phi_i}\right] \tag{5}$$

The linear irregular wave excitation force is then defined as

$$\mathbf{F_e^l} = \Re\left[\sum_{i=1}^{N} \mathbf{H_x}(\omega_i)\eta_{ci}\sqrt{2S(\omega_i)}\Delta\omega_i\right] \tag{6}$$

where $\mathbf{H_x}(\omega) \in \mathbb{C}^{6\times 6}$ is a complex-valued excitation force coefficient that is dependent on the buoy geometry. The excitation force in (6) is calculated around the mean water level, therefore, it does not account for the instantaneous submergence of the buoy, i.e. it is a linearized representation of the actual excitation force around the mean wetted surface. However, it incorporates the forces inserted by the undisturbed incident flow potential and the diffraction potential, i.e.

$$\mathbf{F_e^l} = \mathbf{F_I^l} + \mathbf{F_D} \tag{7}$$

When the instantaneous wetted surface is considered, the incident wave force, the diffracted wave force and the radiated wave force are calculated separately. For a general hull geometry the nonlinear incident wave force, the nonlinear diffracted wave force and the radiated wave force are calculated by computing respectively the surface integral of the pressure due to undisturbed incident wave potential, $P_I(t)$,

$$\mathbf{F_I^{nl}} = -\oiint_{S(t)} P_I(t)\cdot \mathbf{n} dS, \tag{8}$$

the surface integral of the pressure due to the diffracted wave potential, $P_D(t)$,

$$\mathbf{F_D^{nl}} = -\oiint_{S(t)} P_D(t)\cdot \mathbf{n} dS, \tag{9}$$

and the surface integral of the pressure due to the radiated wave potential, $P_R(t)$,

$$\mathbf{F_R^{nl}} = -\oiint_{S(t)} P_R(t)\cdot \mathbf{n} dS \tag{10}$$

over the instantaneous wetted surface, $S(t)$. The surface integral in (8), (9) and (10) can be numerically computed by discretizing the surface of the body with a finite mesh and summing up the forces acting on the area of each panel.

The linear incident wave force, $\mathbf{F_I^l}$, can be found from the nonlinear incident wave force equation simply by assuming the translational and rotational displacement of the buoy to be 0. Since the linear incident wave force does not depend on the displacement of the buoy, it can be pre-computed prior to a simulation.

In [5], it is shown that the nonlinear diffraction and radiation and forces, i.e. the radiation and diffraction forces due to the instantaneous wetted surface, have minor effects on the system dynamics. However, the diffraction force (and the other hydrodynamic forces) needs to be set to 0, when the buoy goes out of the water.

The linear diffraction force or simply the diffraction force, $\mathbf{F_D}$, can be calculated through the diffraction IRF, $\mathbf{K_D}$,

$$\mathbf{F_D} = -\int_{-\infty}^{\infty} \mathbf{K_D}(t-\tau)\eta(\tau)d\tau \tag{11}$$

If the diffraction IRF is not available, one can calculate the nonlinear excitation force as

$$\mathbf{F_e} = \mathbf{F_I^{nl}} - \mathbf{F_I^l} + \mathbf{F_e^l} \tag{12}$$

The linear radiation force or simply the radiation force,$\mathbf{F_r}$, comprises of an inertia and a damping term and is given as

$$\mathbf{F_r} = -\mathbf{M_r}(\omega)\ddot{\mathbf{x}}(t) - \mathbf{R_r}(\omega)\dot{\mathbf{x}}(t) \tag{13}$$

where $\mathbf{M_r}(\omega) \in \mathbb{R}^{6\times 6}$ and $\mathbf{R_r}(\omega) \in \mathbb{R}^{6\times 6}$ are the added mass and radiation damping matrices, respectively, that are dependent on the wave frequency. Cummins [6] showed that the radiation force in (13) could be modelled in time domain as

$$\mathbf{F_r} = -\mathbf{M_r}(\infty)\ddot{\mathbf{x}}(t) - \int_0^t \mathbf{K_r}(t-\tau)\dot{\mathbf{x}}(\tau)d\tau, \tag{14}$$

where $\mathbf{M_r}(\infty) \in \mathbb{R}^{6\times 6}$ is the added mass matrix at infinity frequency and $\mathbf{K_r} \in \mathbb{R}^{6\times 6}$ is the radiation impulse response function. The convolution integral in (14) is computationally expensive, therefore a state-space approximation with n_r number of states is used when dealing with numerical simulations. It can be written as

$$\begin{aligned} \dot{\mathbf{x}}_\mathbf{r}(t) &= \mathbf{A_r}\mathbf{x_r}(t) + \mathbf{B_r}\dot{\mathbf{x}}(t), \quad \mathbf{x_r}(0) = \mathbf{0} \\ \int_{-\infty}^{t} \mathbf{K_r}(t-\tau)\dot{\mathbf{x}}(t)d\tau &\approx \mathbf{C_r}\mathbf{x_r}(t) + \mathbf{D_r}\dot{\mathbf{x}}(t), \end{aligned} \tag{15}$$

where $\mathbf{x_r} \in \mathbb{R}^{n_r\times 1}$ is the radiation state vector $\mathbf{A_r} \in \mathbb{R}^{n_r\times n_r}$, $\mathbf{B_r} \in \mathbb{R}^{n_r\times 6}$, $\mathbf{C_r} \in \mathbb{R}^{6\times n_r}$, $\mathbf{D_r} \in \mathbb{R}^{6\times 6}$ are the time-invariant state, input, output and feedthrough matrices. The system order and the state-space matrices can be found using realization theory, which was proposed by Kung, [7].

The hydrostatic force is equal to the surface integral of the static pressure, $P_{st} = -\rho g z(t)$, over the instantaneous wetted surface, $S(t)$, i.e.

$$\mathbf{F_{hs}} = -\oiint_{S(t)} P_{st}(t)\cdot \mathbf{n} dS \tag{16}$$

The surface integral in (16) can be numerically solved by discretizing the surface of the body with a fine

mesh and summing up the forces acting on the area of each panel. It can also be analytically reformulated, as described in [8],

$$\mathbf{F_{hs}} = \rho g \left(V_{sub}(t) - A_{wp}(t)\eta(t) \right) \mathbf{k} \tag{17}$$

where $V_{sub}(t)$ is the submerged buoy volume, $A_{wp}(t)$ is the water plane area and $\mathbf{k}$ is the vertical unity vector. It must be noted that $\mathbf{F_{hs}}$ is a 6 DoF vector with the last three entries equal to 0, and throughout the text, expressions with unit vectors implies a 6 DoF vector, instead of 3 DoF, with the last three entries equal to 0.

The drag force is proportional to the square of the buoy velocity and it is given as

$$\mathbf{F_{dr}} = -\frac{1}{2}\rho \mathbf{C_d} \mathbf{A_d} \left(\dot{\mathbf{x}}(t) - \mathbf{V_f}(t) \right) \left| \dot{\mathbf{x}}(t) - \mathbf{V_f}(t) \right| \tag{18}$$

where $\mathbf{C_d} \in \mathbb{R}^{6\times6}$ is a diagonal matrix with discharge coefficients, $\mathbf{A_d} \in \mathbb{R}^{6\times6}$ is another diagonal matrix with characteristic areas and $\mathbf{V_f}(t)$ is the fluid particle velocity at the position of the centre of mass of the buoy. It should be noted that drag is defined for translational motion only, but in order to keep all vectors and matrices in 6 DoF, the entries that refer to the rotational states are assigned to 0. The drag coefficient matrix can be obtained by the use of computational fluid dynamic simulations, experimental data and for simple shapes - from handbooks or technical reports.

The gravity force acts in heave and it is constant,

$$\mathbf{F_g} = -m_b g \mathbf{k} \tag{19}$$

The PTO force depends on the type of power take-off and applied control strategy. It is controlled to increase the power capture performance of the buoy. The PTO force will be described in subsequent sections.

In this report, we omit the effect of the mooring loads on the hydrodynamics of the buoy.

D. Heave dynamics

The 6 DoF hydrodynamic model is numerically inefficient due to the high number of states when used in the synthesis of a model predictive control, which is one of the studied control strategies. Since heave is the most important degree of freedom for a point absorber type device, the nonlinear hydrodynamic model only in heave is used to simulate buoy hydrodynamics in this study. Moreover, in order to reduce the complexity of the model predictive control a linearized heave model is derived to be used in the controller design. Since the model is a linearized description of the system, it does not account for the instantaneous submergence of the buoy when calculating the excitation force and other hydrodynamic forces. Therefore, this implies that there will be a mismatch between the plant model and the model that resides inside the controller, when performing the simulations.

The linearized heave model is derived by linearizing the buoy around an operating point, which is chosen to be the center of the buoy. It yields

$$\begin{aligned} m\ddot{z}(t) &= F_e^l + F_{dr}^l + F_r' + F_{hs}^l + F_{pto} + F_g \\ \dot{\mathbf{x}}_\mathbf{r}(t) &= \mathbf{A_r}\mathbf{x_r}(t) + \mathbf{B_r}\dot{z}(t) \\ F_r' &= \mathbf{C_r}\mathbf{x_r}(t) + \mathbf{D_r}\dot{z}(t) \end{aligned} \tag{20}$$

where m is the sum of the buoy mass, m_b, and the added mass at infinity frequency, m_∞. The linearized hydrostatic force is equal to

$$F_{hs}^l = \rho g (V_0 - A_0 z(t)) \tag{21}$$

where V_0 and A_0 are respectively the constant submerged volume and constant water plane area of the buoy at the linearization point.

Due to the fact that the expression for the drag force in (18) is non-smooth at $\dot{z}(t) - \dot{z}_w(t) = 0$, it is not possible to linearize it. However, a linear curve can be constructed that minimizes the error between the actual and the linear curve. For the purpose, the Morison drag linearization technique (see [9]) can be used. It yields

$$F_{dr}^l = -\frac{1}{2}\rho C_d \alpha \Delta\dot{z}_{rms} (\dot{z}(t) - \dot{z}_w(t)), \tag{22}$$

where α is a factor, that is derived to be $\sqrt{8/\pi}$ in [9], and $\Delta\dot{z}_{rms}$ is the root-mean-square (RMS) of the relative velocity. The RMS of the relative velocity equal to $\Delta\dot{z}_{rms} = 0.6m/s$ is found to give sufficiently good approximation in all sea-states.

By rearranging (20), the heave dynamics can be written in state-space form with $n = n_r + 2$,

$$\begin{aligned} \dot{\mathbf{x}}(t) &= \mathbf{A}\mathbf{x}(t) + \mathbf{B}u(t) + \mathbf{B_w}w(t) \\ \mathbf{y}(t) &= \mathbf{C}\mathbf{x}(t) + \mathbf{D}u(t) \end{aligned} \tag{23}$$

where

$$\begin{aligned} \mathbf{x}(t) &= \begin{bmatrix} z(t) & \dot{z}(t) & \mathbf{x_r}^T(t) \end{bmatrix}^T \\ \mathbf{A} &= \begin{bmatrix} 0 & 1 & \mathbf{0}^{1\times n_r} \\ -\dfrac{\rho g A_0}{m} & -\dfrac{1}{m}\mathbf{D_r} & -\dfrac{1}{m}\mathbf{C_r} \\ \mathbf{0}^{n_r\times 1} & \mathbf{B_r} & \mathbf{A_r} \end{bmatrix} \\ \mathbf{B} &= \mathbf{B_w} = \begin{bmatrix} 0 & \dfrac{1}{m} & 0 \end{bmatrix}^T \\ \mathbf{C} &= \begin{bmatrix} \mathbf{I}^{2\times2} & \mathbf{0}^{2\times n_r} \end{bmatrix} \\ \mathbf{D} &= \mathbf{0}^{2\times1} \\ u(t) &= F_{pto} \\ w(t) &= F_e + \rho g V_0 - m_b g + \frac{1}{2}\rho C_d \alpha \Delta\dot{z}_{rms} \dot{z}_w(t) \end{aligned}$$

Note that $w(t)$ is considered as the disturbance turn and it is precomputed prior to simulation. The state-space model of the linearized heave hydrodynamics in (23) is used for the synthesis of the model predictive control.

V. PTO FORCE CONTROL

In this study, three PTO force control strategies are investigated, namely Linear Reactive Control (LRC), Polynomial Reactive Control (PRC) and Nonlinear Model Predictive Control (NMPC). All control strategies have the objective to maximize average export power by considering drivetrain efficiency and constraints. The first two control strategies, LRC and PRC, are non-predictive, i.e. they do not require preview of the wave elevation or wave excitation force. They

incorporate control parameters/features which are optimized for each sea state by using the numerical model of the system. Let us define the feature vector to be $\mathbf{p}$. Hence, the optimization problem is formulated as

$$\begin{aligned} \max_{\mathbf{p}} \quad & \bar{P}_{out}(\mathbf{p}, \mathbf{x}(t), \eta_{pto}, w(t)) \\ \text{s. t.} \quad & \dot{\mathbf{x}}(t) = \mathbf{f}(\mathbf{p}, \mathbf{x}(t), w(t)), \\ & \mathbf{c}(\mathbf{p}, \mathbf{x}(t), w(t)) \leq \mathbf{0} \end{aligned} \tag{24}$$

where η_{pto} is the PTO efficiency. Note that the first term $\dot{\mathbf{x}}(t) = \mathbf{f}(.)$ expressed the system dynamics as an equality constraint and the second term $\mathbf{c}(\mathbf{p}, \mathbf{x}(t), w(t)) \leq \mathbf{0}$ is a generic notation for expressing inequality constraints. We can include the inequality constraint in the objective function using an exterior penalty function $\mathbf{g}(\mathbf{c}(.))$. It yields

$$\begin{aligned} \max_{\mathbf{p}} \quad & \bar{P}_{out}(\mathbf{p}, \mathbf{x}(t), \eta_{pto}, w(t)) - \sigma^T \mathbf{g}\left(\mathbf{c}(\mathbf{p}, \mathbf{x}(t), w(t))\right) \\ \text{s. t.} \quad & \dot{\mathbf{x}}(t) = \mathbf{f}(\mathbf{p}, \mathbf{x}(t), w(t)), \end{aligned} \tag{25}$$

where σ is a penalty coefficient vector. A candidate for a penalty function can be any function that evaluates to 0, if its argument is negative, and to a positive non-decreasing function, if its argument is positive. One such function is the one-sided quadratic function,

$$\mathbf{g}(\mathbf{c}(.)) = min(0, \mathbf{c}(.)^T \mathbf{c}(.)), \tag{26}$$

which is also the one that is used in this study to optimize the feature vectors of LRC and PRC. A simple gradient-based algorithm is implemented in Matlab to solve (25). It is a well-known fact that gradient-based algorithms may lead to a local optimum, instead of a global one, when dealing with non-convex optimization problems, which is the one in (25) due to the nonlinearities in the system dynamics and the objective function. However, if the algorithm is initialized with values that are close to the global optimum solution, the chances of finding the global optimum are high, if the nonlinearity is not that hard. In fact global optimization algorithms are used in conjunction with local optimization algorithms to determine set of initial values for local optimization algorithms. In our case, we will not find optimal parameters in one sea state, but rather to a whole scatter of sea states. Therefore, the optimal value of the neighbouring sea states can be used to initialize the algorithm for any given sea states, assuming that the optimal values of the neighbours are close to the optimum at that sea state, which is true in our case. Therefore, by knowing the optimal values in one sea state, optimal values can be found for the whole scatter with a gradient-based algorithm.

The third control strategy is NMPC, which optimizes the PTO force directly, and not the coefficients of the PTO force as with LRC and PRC, by knowing the incoming wave a few seconds in advance.

The following subsections present the three control strategies in more detail.

E. Linear Reactive Control

Since the very beginning of wave power research, it is a well-known fact that in order to have optimal power absorption, the applied machinery force through the power take-off must comprise of two terms: one that results in reactive power flow and second one that results in an active power transfer. This can simply be achieved by a PTO force that contains a linear spring and a damper term. When motion only in heave is considered, the LRC control law is expressed as

$$F_{pto} = -K_p z(t) - K_v \dot{z}(t) + C \tag{27}$$

where K_p and K_v are respectively PTO spring and damping coefficients, and C is a constant force term to provide pretension. Since InfinityWEC provides the pretension force through the main drivetrain, i.e. without external means such as springs, the constant force term C appears in the total PTO force. The optimal linear PTO spring and damping coefficients can easily be found analytically assuming a linear hydrodynamic buoy model, [10]. However, when the nonlinear force terms and system constraints are considered, the only viable way to find the optimal coefficients is numerically. The gradient-based algorithm is used to solve the optimization problem in (25) with feature/parameter vector

$$\mathbf{p} = \begin{bmatrix} K_p & K_v & C \end{bmatrix}^T. \tag{28}$$

F. Polynomial Reactive Control

PRC can be considered as a higher-order extension of the LRC. The justification for the use of higher-order terms comes from the fact that LRC either amplifies the buoy motion to an extend that system constraints are not satisfied, which makes the implementation of it impractical, or over-dampens the system to satisfy constraints, which causes non-optimal performance. PRC solves the problems of LRC by detuning the reactive force component at higher buoy displacements, thus preventing or minimizing violation of constraints and improving power capture. PRC can be defined mathematically as linear superposition of simple power functions, known also as eigenfunctions, of the position and velocity of the buoy. In the case when only heave motion is considered, the PTO force is

$$\begin{aligned} F_{pto} &= F_p + F_v + C, \\ F_p &= -\sum_{i=1}^{n} a_i z^i(t),\ F_v = -\sum_{j=1}^{m} b_j \dot{z}^j(t). \end{aligned} \tag{29}$$

where a_i and b_j are respectively the polynomial spring and damping coefficients, which can be optimally found by a numerical optimization algorithm, and C is again constant force term for pretension. Due to the fact that the PTO force must be odd symmetric around C, the coefficients with even index can be assigned to 0. The feature vector for polynomial control is

$$\mathbf{p} = \begin{bmatrix} \mathbf{a}^T & \mathbf{b}^T & C \end{bmatrix}^T \tag{30}$$

where $\mathbf{a}$ and $\mathbf{b}$ are vectors respectively with polynomial spring and damping coefficients. It is important to note that the scale of the coefficients is different depending on the power. For example, coefficients in front of higher order terms are lower scale than the coefficients in front of lower order terms. The coefficients must be scaled up or down depending on the order to

have equal scales, which is crucial for the satisfactory operation of the optimization algorithm.

As a side note, generally, linear superposiiton of any eigenfunction, for instance exponentials, can be assigned to the PTO force, to form a different reactive control law.

G. Nonlinear Model Predictive Control

This section describes the mathematical design of a model predictive controller using the linearized model of a wave energy converter. We start by discretizing the linear heave model, derived in (23). It yields,

$$\begin{aligned} \mathbf{x}(k+1) &= \mathbf{A_d}\mathbf{x}(k) + \mathbf{B_d}u(k) + \mathbf{B_{wd}}w(k) \\ \mathbf{y}(k) &= \mathbf{C_d}\mathbf{x}(k) + \mathbf{D_d}u(k) \end{aligned} \tag{31}$$

where $\mathbf{A_d} \in \mathbb{R}^{n\times n}$, $\mathbf{B_d} \in \mathbb{R}^{n\times 1}$, $\mathbf{C_d} \in \mathbb{R}^{2\times n}$ and $\mathbf{D_d} \in \mathbb{R}^{1\times 1}$ are discrete state-space matrices.

The objective is initially defined as direct maximization of the average input power over a period of T seconds. Since optimization algorithms are generally solved as minimization problems, we can define the objective function as minimization of the negative captured power. In discrete time, it is expressed as

$$\min_{u(t)} \quad -\bar{P} = \frac{T_s}{T}\sum_{i=0,\,j=0}^{N-1,\,M-1} v(k+i|k)u(k+j|k), \tag{32}$$

where T_s is the sampling interval, N and M are respectively the prediction and control horizon, v is the discretized buoy velocity and $var(.|k)$ notation is used to indicate that the variable is predicted, i.e. not the measured. At the current time instant $t_0 = kT_s$ the states of the system are measured, hence $x(k|k) = x(k)$. In order to have only variables that can be optimized in the objective function, i.e. not measured, we augment the objective function as

$$\bar{P} = -\frac{T_s}{T}\sum_{i=0,\,j=0}^{N-1,\,M-1} v(k+1+i|k)u(k+j|k), \tag{33}$$

In order to have more design freedom, the objective function is defined in a more general fashion by adding quadratic terms on the outputs and inputs. The system equations are represented as equality constraints and, moreover, inequality constraints on the states and inputs of the system are added. The main design constraints for the PTO in a generic WEC are stroke length, velocity, submerged volume, tether force and rate of change of tether force. For a cylindrical-shaped buoy, the constraint on the submerged volume can be simplified to a constraint on the relative difference between wave elevation and wave position, i.e. the submergence of the buoy, due to the constant waterplane area.

The minimization problem is formulated in matrix notation as

$$\begin{aligned} \min_{\mathbf{Y}_k,\,\mathbf{U}_k} \quad & \frac{1}{2}\mathbf{Y}_k^T\bar{\mathbf{Q}}\mathbf{Y}_k + \frac{1}{2}\mathbf{U}_k^T\bar{\mathbf{R}}\mathbf{U}_k + \mathbf{Y}_k^T\bar{\mathbf{S}}_\mathbf{v}\mathbf{U}_k \\ \text{s. t.} \quad & \mathbf{X}_k = \bar{\mathbf{A}}\mathbf{x}_k + \bar{\mathbf{B}}\mathbf{U}_k + \bar{\mathbf{B}}_\mathbf{w}\mathbf{W}_k \\ & \mathbf{Y}_k = \bar{\mathbf{C}}\mathbf{X}_k + \bar{\mathbf{D}}\mathbf{U}_k \\ & \mathbf{Y_{min}} \le \mathbf{Y}_k \le \mathbf{Y_{max}} \\ & \mathbf{\Delta Z_{min}} \le \bar{\mathbf{S}}_\mathbf{p}^T\mathbf{Y}_k - \mathbf{Z_{w}}_k \le \mathbf{\Delta Z_{max}} \\ & \mathbf{U_{min}} \le \mathbf{U}_k \le \mathbf{U_{max}} \\ & \mathbf{\Delta U_{min}} \le \mathbf{G_{\Delta u}}\mathbf{U}_k + \mathbf{g_{\Delta u}}u_{k-1} \le \mathbf{\Delta U_{max}} \end{aligned} \tag{34}$$

where

$$\begin{aligned} \mathbf{Y}_k &= \begin{bmatrix} \mathbf{y}^T(k+1|k) & \cdots & \mathbf{y}^T(N|k) \end{bmatrix}^T \\ \mathbf{X}_k &= \begin{bmatrix} \mathbf{x}^T(k+1|k) & \cdots & \mathbf{x}^T(N|k) \end{bmatrix}^T \\ \mathbf{U}_k &= \begin{bmatrix} u^T(k|k) & \cdots & u^T(M-1|k) \end{bmatrix}^T \\ \mathbf{W}_k &= \begin{bmatrix} w^T(k|k) & \cdots & w^T(N-1|k) \end{bmatrix}^T \\ \mathbf{Z_{w}}_k &= \begin{bmatrix} z_w^T(k|k) & \cdots & z_w^T(N-1|k) \end{bmatrix}^T \\ \mathbf{Y_{min}} &= \begin{bmatrix} \mathbf{y_{min}}^T & \cdots & \mathbf{y_{min}}^T \end{bmatrix}^T \\ \mathbf{Y_{max}} &= \begin{bmatrix} \mathbf{y_{max}}^T & \cdots & \mathbf{y_{max}}^T \end{bmatrix}^T \\ \mathbf{\Delta Z_{min}} &= \begin{bmatrix} \Delta z_{min}^T & \cdots & \Delta z_{min}^T \end{bmatrix}^T \\ \mathbf{\Delta Z_{max}} &= \begin{bmatrix} \Delta z_{max}^T & \cdots & \Delta z_{max}^T \end{bmatrix}^T \\ \mathbf{U_{min}} &= \begin{bmatrix} u_{min}^T & \cdots & u_{min}^T \end{bmatrix}^T \\ \mathbf{U_{max}} &= \begin{bmatrix} u_{max}^T & \cdots & u_{max}^T \end{bmatrix}^T \\ \mathbf{\Delta U_{min}} &= \begin{bmatrix} \Delta u_{min}^T & \cdots & \Delta u_{min}^T \end{bmatrix}^T \\ \mathbf{\Delta U_{max}} &= \begin{bmatrix} \Delta u_{max}^T & \cdots & \Delta u_{max}^T \end{bmatrix}^T \\ \bar{\mathbf{Q}} &= \mathbf{I}^N \otimes \mathbf{Q} \qquad \mathbf{Q} = diag(q_p,\, q_v) \\ \bar{\mathbf{R}} &= r\mathbf{I}^M \\ \mathbf{S_v} &= \begin{bmatrix} 0 & 1 \end{bmatrix}^T \qquad \mathbf{S_p} = \begin{bmatrix} 1 & 0 \end{bmatrix}^T \\ \bar{\mathbf{S}}_\mathbf{v} &= \begin{cases} \mathbf{I}^N \otimes \mathbf{S_v} & \text{, if } M = N \\ \begin{bmatrix} \mathbf{I}^M \otimes \mathbf{S_v} \\ {\mathbf{S_v}}^{NM} \end{bmatrix} & \text{, if } M < N \end{cases} \\ {\mathbf{S_v}}^{NM} &= \begin{bmatrix} \mathbf{0} & \cdots & \mathbf{0} & \mathbf{S_v} \\ \vdots & \ddots & \vdots & \vdots \\ \mathbf{0} & \cdots & \mathbf{0} & \mathbf{S_v} \end{bmatrix} \\ \bar{\mathbf{S}}_\mathbf{p} &= \mathbf{I}^N \otimes \mathbf{S_p} \\ \bar{\mathbf{A}} &= \begin{bmatrix} {\mathbf{A_d}}^T & {\mathbf{A_d}}^{2T} & \cdots & {\mathbf{A_d}}^{NT} \end{bmatrix}^T \\ \bar{\mathbf{B}} &= \begin{bmatrix} \mathbf{B_d} & \mathbf{0} & \cdots & \mathbf{0} \\ \mathbf{A_d}\mathbf{B_d} & \mathbf{B_d} & \cdots & \mathbf{0} \\ \vdots & \vdots & \ddots & \vdots \\ {\mathbf{A_d}}^{M-1}\mathbf{B_d} & {\mathbf{A_d}}^{M-2}\mathbf{B_d} & \cdots & \mathbf{B_d} \\ {\mathbf{A_d}}^{M}\mathbf{B_d} & {\mathbf{A_d}}^{M-1}\mathbf{B_d} & \cdots & (\mathbf{A_d}+\mathbf{I})\mathbf{B_d} \\ \vdots & \vdots & \ddots & \vdots \\ {\mathbf{A_d}}^{N-1}\mathbf{B_d} & {\mathbf{A_d}}^{N-2}\mathbf{B_d} & \cdots & \sum_{i=0}^{N-M}{\mathbf{A_d}}^{i}\mathbf{B_d} \end{bmatrix} \\ \bar{\mathbf{B}}_\mathbf{w} &= \begin{bmatrix} \mathbf{B_{wd}} & \mathbf{0} & \cdots & \mathbf{0} \\ \mathbf{A_d}\mathbf{B_{wd}} & \mathbf{B_{wd}} & \cdots & \mathbf{0} \\ \vdots & \vdots & \ddots & \vdots \\ {\mathbf{A_d}}^{N-1}\mathbf{B_{wd}} & {\mathbf{A_d}}^{N-2}\mathbf{B_{wd}} & \cdots & \mathbf{B_{wd}} \end{bmatrix} \\ \bar{\mathbf{C}} &= \mathbf{I}^N \otimes \mathbf{C_d} \\ \bar{\mathbf{D}} &= \mathbf{I}^N \otimes \mathbf{D_d} \\ \mathbf{g_{\Delta u}} &= \begin{bmatrix} -1 & 0 & \cdots & 0 \end{bmatrix}^T \end{aligned}$$

$$\mathbf{G_{\Delta u}} = \begin{bmatrix} 1 & 0 & \cdots & 0 \\ -1 & 1 & \cdots & 0 \\ \vdots & \ddots & \ddots & \vdots \\ 0 & \cdots & -1 & 1 \end{bmatrix}$$

q_p – quadratic penalty of position
q_v – quadratic penalty of velocity
r – quadratic penalty of input force

Substituting the equality constraints in the objective functions in (34), yields

$$\begin{aligned} \min_{\mathbf{U}_k} \quad & \frac{1}{2}\mathbf{U}_k^T\mathbf{H}\mathbf{U}_k + \mathbf{f}_k^T\mathbf{U}_k \\ \text{s. t.} \quad & \mathbf{G}\mathbf{U}_k \leq \mathbf{h}_k \end{aligned} \tag{35}$$

where

$$\begin{aligned} \mathbf{H} &= \mathbf{G_y}^T\left(\bar{\mathbf{Q}}\mathbf{G_y} + \bar{\mathbf{S}}_\mathbf{v}\right) + \bar{\mathbf{R}} \\ \mathbf{G_y} &= \bar{\mathbf{C}}\bar{\mathbf{B}} + \bar{\mathbf{D}} \\ \mathbf{f}_k &= \bar{\mathbf{W}}_\mathbf{k}^T\left(\bar{\mathbf{Q}}\mathbf{G_y} + \bar{\mathbf{S}}_\mathbf{v}\right) \\ \bar{\mathbf{W}}_\mathbf{k} &= \bar{\mathbf{C}}(\bar{\mathbf{A}}\mathbf{x}_k + \bar{\mathbf{B}}_\mathbf{w}\mathbf{W}_k) \end{aligned}$$

$$\mathbf{G} = \begin{bmatrix} \mathbf{G_y} \\ -\mathbf{G_y} \\ \bar{\mathbf{S}}_\mathbf{p}^T\mathbf{G_y} \\ -\bar{\mathbf{S}}_\mathbf{p}^T\mathbf{G_y} \\ \mathbf{I}^{M\times M} \\ -\mathbf{I}^{M\times M} \\ \mathbf{G_{\Delta u}} \\ -\mathbf{G_{\Delta u}} \end{bmatrix} \quad \mathbf{h}_k = \begin{bmatrix} \mathbf{Y_{max}} - \bar{\mathbf{W}}_\mathbf{k} \\ -\mathbf{Y_{min}} + \bar{\mathbf{W}}_\mathbf{k} \\ \mathbf{\Delta Z_{max}} - \bar{\mathbf{S}}_\mathbf{p}^T\bar{\mathbf{W}}_\mathbf{k} + \mathbf{Z_w} \\ -\mathbf{\Delta Z_{min}} + \bar{\mathbf{S}}_\mathbf{p}^T\bar{\mathbf{W}}_\mathbf{k} - \mathbf{Z_w} \\ \mathbf{U_{max}} \\ -\mathbf{U_{min}} \\ \mathbf{\Delta U_{max}} - \mathbf{g_{\Delta u}}u_{k-1} \\ -\mathbf{\Delta U_{min}} + \mathbf{g_{\Delta u}}u_{k-1} \end{bmatrix}$$

If the constraints that are enforced on the system are too strict, the optimization algorithm might fail to find an optimal solution in the feasible set. At such scenario the optimization will not give any control input, i.e. the system will run in open loop. Therefore, we need to find a way to handle these situations. One of the most common ways is softening the constraints by introducing slack variables in the optimization problem. We define the new control problem as

$$\begin{aligned} \min_{\mathbf{Y}_k,\,\mathbf{U}_k,\,\epsilon_k} \quad & \frac{1}{2}\mathbf{Y}_k^T\bar{\mathbf{Q}}\mathbf{Y}_k + \frac{1}{2}\mathbf{U}_k^T\bar{\mathbf{R}}\mathbf{U}_k + \mathbf{Y}_k^T\bar{\mathbf{S}}_\mathbf{v}\mathbf{U}_k \\ & + \frac{1}{2}\epsilon_k^T\mathbf{P}\epsilon_k + \mathbf{p}^T\epsilon_k \\ \text{s. t.} \quad & \mathbf{X}_k = \bar{\mathbf{A}}\mathbf{x}_k + \bar{\mathbf{B}}\mathbf{U}_k + \bar{\mathbf{B}}_\mathbf{w}\mathbf{W}_k \\ & \mathbf{Y}_k = \bar{\mathbf{C}}\mathbf{X}_k + \bar{\mathbf{D}}\mathbf{U}_k \\ & \mathbf{Y}_k \leq \mathbf{Y_{max}} + \mathbf{V_{y_{max}}}\epsilon_\mathbf{y} \\ & -\mathbf{Y}_k \leq -\mathbf{Y_{min}} + \mathbf{V_{y_{min}}}\epsilon_\mathbf{y} \\ & \bar{\mathbf{S}}_\mathbf{p}^T\mathbf{Y}_k \leq \mathbf{\Delta Z_{max}} + \mathbf{V_{\Delta z_{max}}}\epsilon_\mathbf{\Delta z} + \mathbf{Z_w}_k \\ & -\bar{\mathbf{S}}_\mathbf{p}^T\mathbf{Y}_k \leq -\mathbf{Z_{min}} + \mathbf{V_{\Delta z_{min}}}\epsilon_\mathbf{\Delta z} - \mathbf{Z_w}_k \\ & \mathbf{U}_k \leq \mathbf{U_{max}} + \mathbf{V_{u_{max}}}\epsilon_\mathbf{u} \\ & -\mathbf{U}_k \leq -\mathbf{U_{min}} + \mathbf{V_{u_{min}}}\epsilon_\mathbf{u} \\ & \mathbf{G_{\Delta u}}\mathbf{U}_k \leq \mathbf{\Delta U_{max}} + \mathbf{V_{\Delta u_{max}}}\epsilon_\mathbf{\Delta u} - \mathbf{g_{\Delta u}}u_{k-1} \\ & -\mathbf{G_{\Delta u}}\mathbf{U}_k \leq -\mathbf{\Delta U_{min}} + \mathbf{V_{\Delta u_{min}}}\epsilon_\mathbf{\Delta u} + \mathbf{g_{\Delta u}}u_{k-1} \\ & -\epsilon_k \leq \mathbf{0}^{5\times 1} \end{aligned} \tag{36}$$

where

$$\epsilon = \begin{bmatrix} \epsilon_p & \epsilon_v & \epsilon_{\Delta z} & \epsilon_u & \epsilon_{\Delta u} \end{bmatrix}^T$$

is a vector with slack variables for each constraint,

$$\mathbf{P} = diag(\rho_p,\ \rho_v,\ \rho_{\Delta z},\ \rho_u,\ \rho_{\Delta u}),$$
$$\mathbf{p} = \begin{bmatrix} \sigma_p & \sigma_v & \sigma_{\Delta z} & \sigma_u & \sigma_{\Delta u} \end{bmatrix}^T$$

are the weights for each slack variable respectively for the quadratic and linear penalty function, and

$$\mathbf{V_y} = \begin{bmatrix} \mathbf{V_{y_{max}}} \\ \mathbf{V_{y_{min}}} \end{bmatrix} = \begin{bmatrix} V_{y_p max} & 0 \\ 0 & V_{y_v max} \\ \vdots & \vdots \\ V_{y_p max} & 0 \\ 0 & V_{y_v max} \\ V_{y_p min} & 0 \\ 0 & V_{y_v min} \\ \vdots & \vdots \\ V_{y_p min} & 0 \\ 0 & V_{y_v min} \end{bmatrix}$$

$$\mathbf{V_{\Delta z}} = \begin{bmatrix} \mathbf{V_{\Delta z_{max}}} \\ \mathbf{V_{\Delta z_{min}}} \end{bmatrix} = \begin{bmatrix} V_{\Delta z max} \\ \vdots \\ V_{\Delta z max} \\ V_{\Delta z min} \\ \vdots \\ V_{\Delta z min} \end{bmatrix}$$

$$\mathbf{V_u} = \begin{bmatrix} \mathbf{V_{u_{max}}} \\ \mathbf{V_{u_{min}}} \end{bmatrix} = \begin{bmatrix} V_{u max} \\ \vdots \\ V_{u max} \\ V_{u min} \\ \vdots \\ V_{u min} \end{bmatrix}$$

$$\mathbf{V_{\Delta u}} = \begin{bmatrix} \mathbf{V_{\Delta u_{max}}} \\ \mathbf{V_{\Delta u_{min}}} \end{bmatrix} = \begin{bmatrix} V_{\Delta u max} \\ \vdots \\ V_{\Delta u max} \\ V_{\Delta u min} \\ \vdots \\ V_{\Delta u min} \end{bmatrix}$$

are matrices with non-negative entries, where the larger the entry in the matrix, the relatively softer the corresponding constraints is. Again substituting the equality constraints in the objective function and the inequality constraints, we obtain the optimization problem in terms of the control inputs and slack variables,

$$\begin{aligned} \underset{\bar{\mathbf{U}}_k}{\text{minimize}} \quad & \frac{1}{2}\bar{\mathbf{U}}_k^T\bar{\mathbf{H}}\bar{\mathbf{U}}_k + \bar{\mathbf{f}}_k^T\bar{\mathbf{U}}_k \\ \text{subject to} \quad & \bar{\mathbf{G}}\bar{\mathbf{U}}_k \leq \bar{\mathbf{h}}_k \end{aligned} \tag{37}$$

where

$$\bar{\mathbf{H}} = \begin{bmatrix} \mathbf{H} & \mathbf{0} \\ \mathbf{0} & \mathbf{P} \end{bmatrix} \qquad \bar{\mathbf{f}}_k = \begin{bmatrix} \mathbf{f}_k^T & \mathbf{p}^T \end{bmatrix}^T$$
$$\bar{\mathbf{G}} = \begin{bmatrix} \mathbf{G} & -\mathbf{V} \\ \mathbf{0}^{5\times M} & -\mathbf{I}^5 \end{bmatrix} \quad \bar{\mathbf{h}}_k = \begin{bmatrix} \mathbf{h}_k \\ \mathbf{0}^{5\times 1} \end{bmatrix}$$
$$\mathbf{V} = blkdiag(\mathbf{V_y}, \mathbf{V_{\Delta z}}, \mathbf{V_u}, \mathbf{V_{\Delta u}})$$

The optimization problem in (37) is a convex one, for which powerful convex optimization algorithms are available that can solve the problem in real time.

However, its solution maximizes the captured power of the wave energy converter, i.e. it does not consider the losses in the power take-off. Not accounting for the losses in the drivetrain leads to large reciprocating power flows, thus, causing increased losses and reduced output power as an end result. On the contrary, by maximization of the output power instead, i.e. by accounting for the efficiency of the PTO, the optimal balance between captured and returned power is achieved. The optimization problem that maximizes the output power (minimizes the negative of the output power) can be expressed in continuous time as

$$\underset{u(t)}{\text{minimize}} \quad -\bar{P}_o(t) = \frac{1}{T}\int_{t_0}^{t_0+T} \dot{z}(t)u(t)\eta_{PTO}(t)dt \quad (38)$$

where η_{PTO} is the PTO efficiency,

$$\eta_{PTO}(t) = \begin{cases} \eta_0, & \text{if } \dot{z}(t)u(t) \leq 0 \\ \dfrac{1}{\eta_0}, & \text{otherwise} \end{cases} \quad (39)$$

The efficiency function in (39) can be smoothed with the logistic function

$$\eta_{PTO_{smooth}}(t) = \frac{\eta_0 + \dfrac{1}{\eta_0}e^{\gamma p(t)}}{1 + \dfrac{1}{\eta_0}e^{\gamma p(t)}}, \quad (40)$$

where $p(t) = \dot{z}(t)u(t)$ and γ is a measure of the steepness of the transition from one efficiency level to another, and

$$\lim_{\gamma\to\infty} \eta_{PTO_{smooth}}(t) = \eta_{PTO}(t). \quad (41)$$

This objective function makes the optimization problem non-convex, therefore, making the control problem harder to solve. A simple way to account for them, while preserving the convexity of the problem is to assume that the losses are viscous. We modify the performance objective accordingly

$$\underset{u(t)}{\text{minimize}} \quad \bar{P}_o(t) = \frac{1}{T}\int_{t_0}^{t_0+T} \dot{z}(t)u(t) + b_v\dot{z}^2 dt \quad (42)$$

where b_v is a non-negative viscous friction coefficient, which needs to be optimized for maximum output power using Monte Carlo simulations for each sea state. This modification does not change the already derived control problem. We just need to change the second diagonal entry in the output weighing vector $\mathbf{Q} = diag(q_p, q_v)$ to equal to b_v, i.e. $q_v = b_v$.

VI. Implementation

The open-source Boundery Element Method (BEM) solver Nemoh, [11], is used to generate the hydrodynamic parameters of the WEC. The process starts by creating a mesh of the cylindrical hull. Then the generated mesh file is fed as input to the mesh routine of Nemoh along with environmental parameter, such as water depth and wave direction to generate the hydrodynamic coefficients. The hydrodynamic parameters of the cylindrical hull are summarized in Table IV.

TABLE IV
Constant hydrodynamic coefficients of the cylindrical buoy in heave.

Symbol	Quantity	Value	Unit
m_∞	Added mass	649.1[a]	ton
k_h	Hydrostatic stiffness	1.78[a]	MN/m
C_d	Drag coefficient	1.15[b]	-

[a] The added mass and the hydrostatic stiffness are calculated using Nemoh .
[b] The value of the drag coefficient is set according to DNV Standards, [12], for an oscillatory wave scenario.

In order to conduct the time domain simulations, the nonlinear hydrodynamic model of the cylindrical buoy in heave is implemented in Simulink/MATLAB along with the three control strategies. The irregular waves are produced with the JONSWAP wave distribution model with steepness coefficient of $\gamma = 3.3$. Simulations are run using the ode45 solver with maximum time step of 0.01s. The simulation duration is set to 2 hours for all simulations and each control strategy is simulated with the same wave timeseries to obtain comparable results.

The design constraints of the wave energy converter are stroke length, velocity, tether force, rate of change of control/tether force and buoy volume/submergence. The constraints of the studied controllers, which are summarized in Table V, are chosen accordingly. Note

TABLE V
Design constraints of the studied wave energy converter

Symbol	Quantity	Value	Unit
z_{max}	Maximum buoy displacement	2.5	m
z_{min}	Minimum buoy displacement	-2.5	m
$\dot{z}_{max}$	Maximum buoy velocity	2.0	m/s
$\dot{z}_{min}$	Minimum buoy velocity	-2.0	m/s
Δz_{max}	Maximum submergence	1.23	m
Δz_{min}	Minimum submergence	-1.23	m
u_{max}	Maximum tether force	0.0	MN
u_{min}	Minimum tether force	-3.0	MN
Δu_{max}	Maximum rate of control	10.0	MN/s
Δu_{min}	Minimum rate of control	-10.0	MN/s

that the constraint on the rate of change is set to a high value, meaning that it will be disabled in this study. Moreover, it will be assumed that the size of the storage is large enough so that it smooths the input power to a constant level, equal to the average for each sea state. Since the average export power is unknown prior to simulation and there is no dynamic model of the machinery, the power at each node of the power take-off cannot be calculated during simulation. Therefore, they will be found by postprocessing the input power to the PTO using the efficiency of each component. In order to calculate the average output power correctly, energy neutrality of the storage must be guaranteed, meaning that the stored energy in the flywheel at the beginning of the simulation must be equal to the stored

energy at the end of the simulation. This way any bias in the average output power due to the storage is eliminated.

In order to keep the number of optimized parameters low, a third-order polynomial is used in this study. The penalty coefficient in the objective function of the optimization problem of LRC and PRC is chosen to be $\sigma = 20$ for all constraints. While performing simulations with LRC and PRC, it was observed that the controllers performed poorly at keeping the tether force constraint. Therefore, in order to have more fair comparison against results with NMPC, the output of the controller was saturated with the boundaries of the tether force constraint.

The MPC with the non-convex objective and smooth efficiency function is used. The optimization problem of the controller is solved with the fmincon function in Matlab with the SQP (Sequential Quadratic Programming) algorithm. The used parameters of the controller are summarized as follows

$$\begin{aligned} N &= M = 50 \\ T_s &= 0.1s \\ \gamma &= 40 \\ \eta_0 &= 0.841 \\ \mathbf{P} &= 1e4 \times \mathbf{I}^5 \\ \mathbf{p} &= \mathbf{0}^{5\times 1} \\ V_{y_p max} = V_{y_v min} &= V_{y_p max} = V_{y_v min} = 1.0 \\ V_{\Delta z max} &= V_{\Delta z min} = 0.1 \\ V_{u max} &= V_{u min} = 0.1 \\ V_{\Delta u max} &= V_{\Delta u min} = 1.0 \end{aligned}$$

Note that 50-step prediction horizon with 0.1s sampling time corresponds to 5s prediction time. The efficiency η_0 is found by multiplying all the efficiency values of all components in Table II, but the efficiency value of the output inverter, since the power flow through the output inverter is only in one direction, i.e. it does not participate in the reactive power transfer. The submergence and the tether force constraints are designed to be harder compared to stroke and velocity constraints. Submergence constraint is chosen to be harder to prevent occurrence of strong model nonlinearity due to going-out and completely submerging of the buoy, which can cause instability. The motivation behind choosing the tether force constraint to be harder is due to the fact that force is the most critical design parameter for the machinery. The

VII. Simulation results

H. Single sea state benchmark

In this subsection the studied control strategies are benchmarked in a single sea state, namely $H_s = 5.0m$, $Tp = 10.4s$. The comparison is summarized in Table VI.

As expected, the NMPC outperforms the other control strategies in terms of mean export power, followed by the PRC. However, NMPC is not the winner in terms of wave-to-wire efficiency due to the relatively high average tether power. The NMPC outperforms the other two control strategies in a remarkable way in terms of control handling capability, which can be understood by looking at the peak tether power. The constraint management with PRC is better than LRC but the difference is not that significant. Finally, the NMPC requires lower storage capacity to achieve constant output power compared to the other two passive control strategies. It should be noted that PRC has outperformed the LRC in all categories in the chosen sea state.

TABLE VI
BENCHMARK IN HS=5.0M TP=10.4S

Quantity	LRC	PRC	NMPC	Unit
Mean export power	345	427	475	kW
Mean tether power	439	563	623	kW
Wave-to-wire efficiency	78.6	75.8	76.2	%
Peak tether power	8.9	8.4	6.3	MW
Pta tether power	20.3	15.0	10.1	-
Utilized storage capacity	41	39	34	kWh

I. Annual benchmark

In this section the three control strategies are benchmarked based on annual data. The results with LRC and PRC are obtained by optimally tuning their control coefficients for each sea state. Fig. 5 shows the averaged export power and the statistical peak tether power for the studied control strategies. It can be clearly seen that NMPC can achieve the highest average output power in all sea states, while requiring the lowest peak tether power. Although, it performs best at minimizing the peak tether power, it fails at keeping the tether power below the defined 6MW boundary at the largest sea states. From Fig. 5, it can be seen that LRC is the worst performer in all sea states in terms average export power and peak tether power. The difference in performance between LRC and the other control strategies is more visible in the largest sea states. In largest sea states, LRC causes the maximum allowed tether power to be exceeded almost two times.

Fig. 6 shows direct comparison of the constraint handling capability of each control strategy by showing the utilized stroke length and maximum velocity at each sea state in the selected site. By looking at the maximum stroke scatters in Fig. 6, it can be seen that all control strategies have significantly violated the chosen constraint. The reason for this can be that the penalty for the violation of the stoke constraint was not large enough. In case of NMPC the reason is also partially due to the mismatch between the plant and controller model. Increasing the penalty on violation of the stroke constraint might improve the case. However, this improvement only be achieved at the expense of violating another constraint, such as the velocity.

Fig. 6, furthermore, shows that the velocity constraint is much less violated, with the best result for NMPC. Velocity is less critical than stroke length for the PTO, which indicates that the softness parameter

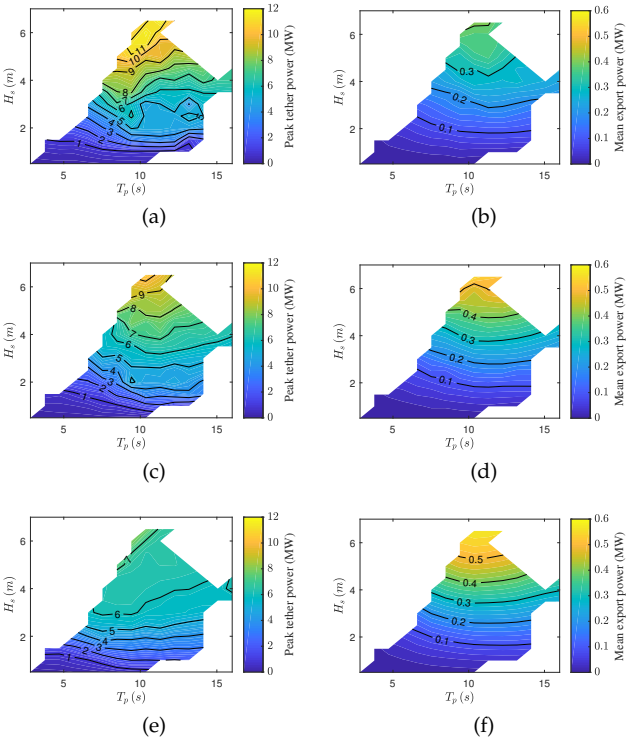

Fig. 5. Power matrices obtained for LRC (first row), PRC (second row) and NMPC (third row). Left column shows peak tether powers, while right column shows mean export power. The controller parameters of LRC and PRC are optimized at each sea state.

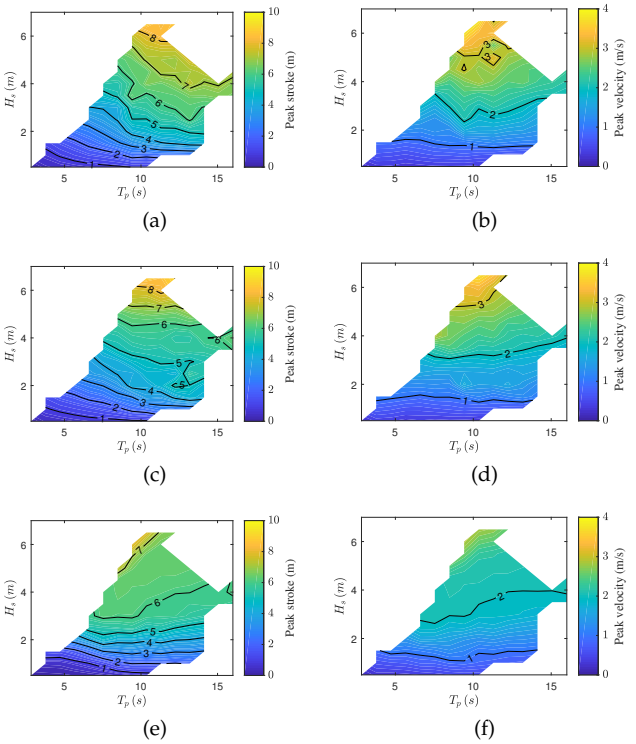

Fig. 6. Peak statistical values of stroke and velocity obtained for LRC (first row), PRC (second row) and NMPC (third row). Left column shows peak stroke length, while right column shows peak velocity. The controller parameters of LRC and PRC are optimized at each sea state.

could be changed to allow more violation. Due to time limitation in this study, the constraint handling capability could not be tested for different softness parameters of the NMPC. Therefore, one potential future task can be to measure violation of constraints for different softness parameters. It should be also noted that power has not been used as a constraint in this study, which means that the velocity constraint limits the peak power in the system. Therefore, another potential future work is to implement a constraint for the power, to allow higher velocity when the force is lower.

LRC and PRC were simulated with higher values of the penalty weight, σ. However, the constraint violations did not reduce much and it even got much worse in some occasions, indicating that the utilized gradient-based optimization algorithm failed to find an optimal solution due to the hardening the nonlinearity of the objective function. Therefore, the utilized gradient-based algorithm is not suitable for problems with large constraint penalty coefficients. In a future study, global optimization algorithms such as genetic algorithm or particle swarm algorithm can be used to find the optimal controller coefficients.

A thorough performance benchmark based on annual wave scatter between the three control strategies is summarized in Table VII. NMPC is able to export 17.4% more annual energy compared PRC and 28% more - compared to LRC. PRC is 9% better than LRC in terms of export power. Similar to the single sea state case, the wave-to-wire efficiency with PRC is observed to be slightly better than NMPC and LRC when annual data is considered. Annual mean RMS

TABLE VII
BENCHMARK BASED ON ANNUAL DATA

Quantity	LRC	PRC	NMPC	Unit
Annual export energy	1.00	1.09	1.28	GWh
Mean annual export power	117	127	149	kW
Annual tether energy	1.36	1.48	1.74	GWh
Mean annual tether power	159	173	203	kW
Wave-to-wire efficiency	73.7	73.2	73.3	%
Peak tether force	3.0	3.0	3.0	MN
Annual mean RMS tether force	0.80	0.83	1.11	MN
Mean exp. power/RMS teth. force	147	152	135	W/kN
Mean exp. power/Peak teth. force	39	42	50	W/kN
Flywheel in-out energy volume	2.03	2.26	2.92	GWh
Nr of cycles/10kWh storage in 20y	2.0m	2.3m	2.9m	-

tether force on the table refers to the weighted average of the RMS tether force by the occurrence of each sea state in the selected site. It can be seen that LRC has the lowest RMS tether force. This implies better load case for the LRC compared to the other control strategies. However, this also implies reduced utilization of the available peak force. Although, LRC has the lowest annual mean RMS tether force and NMPC has the highest mean annual export power, the winner in terms of mean export power per RMS tether force is PRC. However, if the mean export power per peak tether force is considered, the NMPC outperforms the passive control strategies. However, it is unknown whether mean power per RMS or mean power per peak force is the cost-defining metric. Therefore, it is difficult to

say which control strategy is better in terms of cost.

In this study, the storage requirement for each control strategy is also analyzed. The penultimate row in Table VII shows the exchanged energy volume, that flows into and out from the storage device for one year. It can be clearly seen that NMPC causes significantly higher power flow through the flywheel, while the exchanged energy volume with PRC is slightly higher than LRC. The exchanged energy volume is an important quantity, since it is directly proportional to the number of full charge-discharge cycles per KWh of storage capacity of the flywheel, which is depicted in the last row of the table. Therefore, similarly, the LRC requires slightly (13%) lower number of cycles compared to PRC and significantly (46%) lower compared to NMPC.

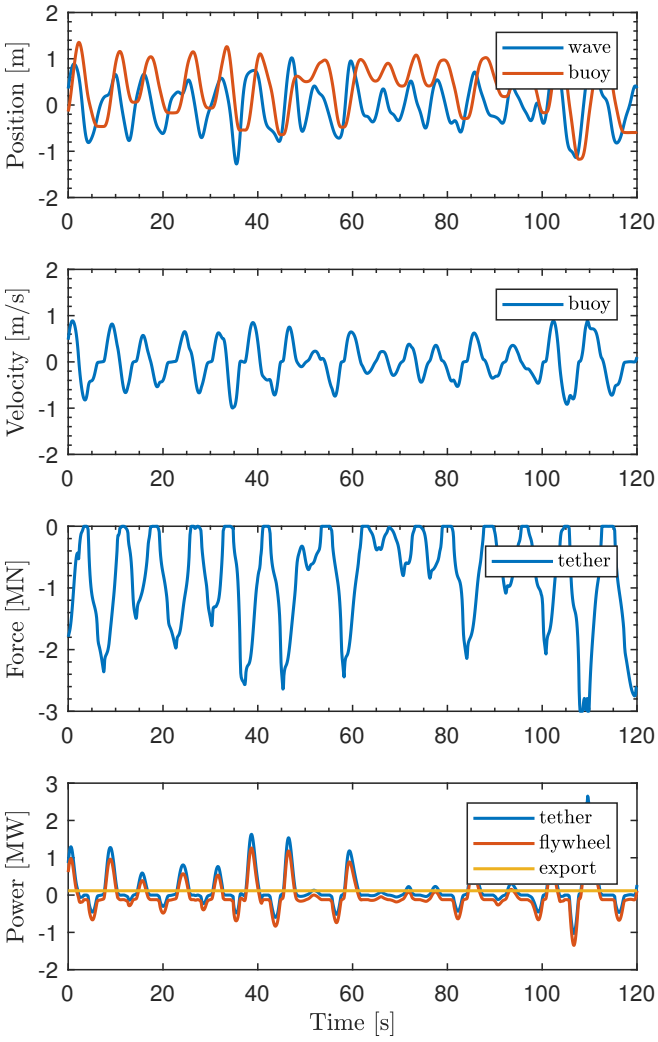

Fig. 7. Timeseries in sea state $H_s = 2.0m$, $T_P = 8.5s$ with NMPC.

J. Hydrodynamic behaviour with NMPC

Figure 7 and 8 display the timeseries of some of the main signals, obtained by simulating the studied buoy with the NMPC in two selected sea states, namely at $H_s = 2.0m$, $T_p = 8.5s$ and $H_s = 5.0m$, $T_p = 10.4s$.

It can be seen that the NMPC manages to control the buoy without any violation of the system constraints in the small sea state, and with some small violations in the larger one. Moreover, by looking at the tether force curve in the smaller sea state, the efficiency awareness of the controller can be noted. The NMPC keeps the tether force low in order to increase the output power. If the controller was designed without accounting for the efficiency of the system, then it would have utilized higher tether force, which would lead to higher power capture, but also higher reciprocating power flows causing increased losses and, therefore, lower output power as an end result. Using a lower average tether force or lower pretension force in small sea states has a consequence, though. The buoy does not operate around the point, at which it was linearized, i.e. the center of the cylinder. It can be seen by looking at the wave and buoy position in the top subplot of Fig. 7 that the mean buoy position is higher than the mean wave elevation and/or the position of (the center of) the buoy is most of the time above the water surface. Therefore, in small sea states the mismatch between the nonlinear plant model and the linearized controller model increases, which can have a deteriorating effect on the performance of the controller. In our particular case, the buoy is quite short, thus, the difference between the nonlinear and linear excitation force is small due to the small draft of the buoy. The difference is expected to be greater with taller and narrower buoys.

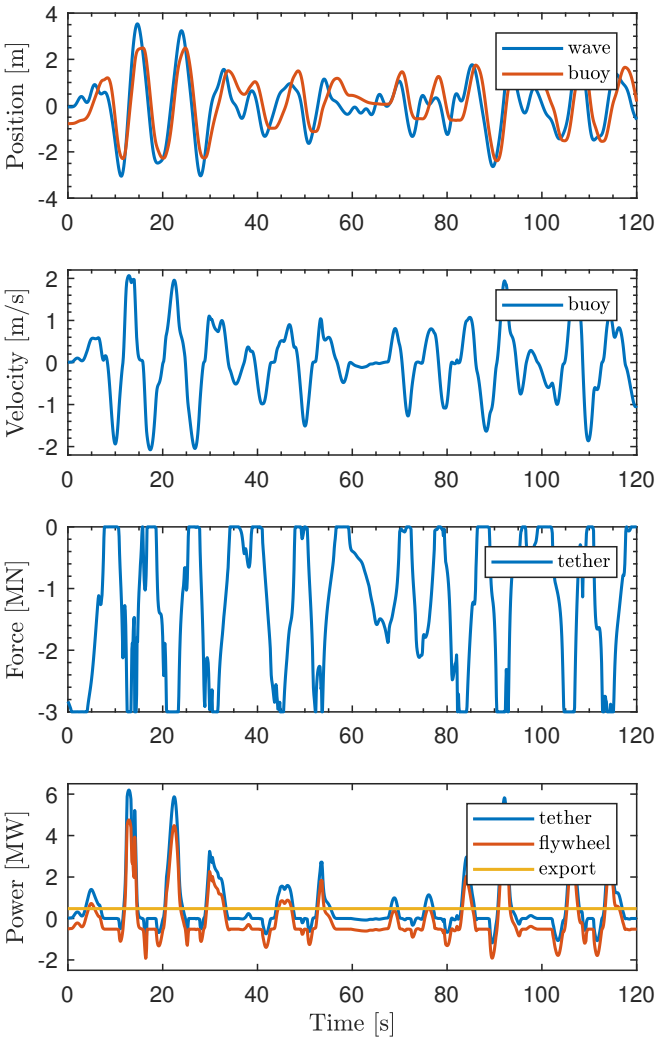

Fig. 8. Timeseries in sea state $H_s = 5.0m$, $T_P = 10.4s$ with NMPC.

The efficiency awareness of the controller can also be noted by looking at the power curves in both figures. It can be seen that the returned power to the buoy is much smaller than the captured power.

VIII. Conclusions

This paper presented a benchmarking study of the InfinityWEC wave energy converter, where three different efficiency-aware reactive control techniques, namely linear reactive control (LRC), polynomial reactive control (PRC) and nonlinear model predictive control (NMPC) are compared in terms of performance, load case and constraint handling capability.

As anticipated, the NMPC resulted in highest annual energy yield, using 5s prediction of wave input, due to its more detailed control capability: 17.4% higher than PRC and 28% higher than LRC. Without prediction of wave input, PRC performed 9% better in terms of annual energy compared to the LRC due to the higher degree of flexibility of the polynomial controller to handle constraints in a more optimal way, mainly, in larger sea states. In more energetic sites the improvement with PRC with respect to LRC is expected to be higher. However, performance of the control strategies relative to one another also depends on the chosen system constraints. For example, if the limits of the system are sufficiently high, then the optimal coefficients of the PRC will be equal to the ones of the LRC, thus, there will be no improvement.

The annual mean RMS and the peak tether force was used in this study to describe the load case for the different control strategies. The peak tether force is saturated at 3MN for each control strategy. LRC is found to have the lowest annual mean RMS tether force, implying that it has better load case in terms of RMS compared to other two control strategies. However, lower RMS force also means lower utilization of the available peak tether force. In order to obtain some sense on the system performance in relation to the load case and/or utilization, the mean annual export power per peak tether force and mean annual export power per RMS tether force are calculated. It was found that NMPC yields highest annual mean export power per peak tether force, as expected. However, the PRC offers the best performance per RMS tether force. This implies that PRC may be the most cost-effective control strategy.

LRC was found to have the lowest utilization of the storage with 13% and 46% less exchanged energy volume in and out from the flywheel compared to respectively PRC and NMPC. This implies that lower number of full charge-discharge cycles per kWh storage capacity is required with the LRC. However, from the single sea state simulation it was found that LRC utilizes the highest storage capacity.

In terms of constraint handling capability, NMPC outperforms both passive control strategies followed by PRC, as anticipated. However, the chosen softening parameters for NMPC did not yield satisfactory constraint handling capability on all of the state variables. For example, the NMPC performed quite satisfactorily in keeping the velocity constraint, but great violations of the stroke constraint were observed, implying that the stroke constraint could be hardened by decreasing the value of the corresponding softening parameter. Although, simulations were not run for different sets of softening parameters, it is anticipated that hardening the constraint of one of the state variables is in the expense of softening, thus, increasing the violations of the other due to the maximum available force input.

The justification for the poor performance of LRC and PRC can be argued to be in the choice of insufficient penalty weights. However, the gradient-based optimization algorithm, utilized in this study to find optimal control coefficients of the passive control techniques, failed to work properly for higher values of the penalty coefficients. It is anticipated that violations can be reduced by hardening the constraints with higher constraint weights. However, this will be in the expense of output power performance of the device.

References

[1] M. Hannon, J. Griffiths, A. Vantoch-Wood, M. Carcas, S. Bradley, R. Boud, and S. Wyatt, "Marine energy (world energy resources 2016)," Tech. Rep., 2016.

[2] N. Sergiienko, A. Rafiee, B. Cazzolato, B. Ding, and M. Arjomandi, "Feasibility study of the three-tether axisymmetric wave energy converter," *Ocean Engineering*, vol. 150, pp. 221 – 233, 2018. [Online]. Available: http://www.sciencedirect.com/science/article/pii/S002980181730793X

[3] A. Babarit, J. Hals, M. J. Muliawan, A. Kurniawan, T. Moan, and J. Krokstad, "Numerical benchmarking study of a selection of wave energy converters," *Renewable Energy*, vol. 41, pp. 44–63, 2012. [Online]. Available: http://www.sciencedirect.com/science/article/pii/S0960148111005672

[4] A. De Andres, J. Maillet, J. Hals Todalshaug, P. Möller, D. Bould, and H. Jeffrey, "Techno-economic related metrics for a wave energy converters feasibility assessment," *Sustainability*, vol. 8, no. 11, 2016. [Online]. Available: http://www.mdpi.com/2071-1050/8/11/1109

[5] A. Merigaud, J. C. Gilloteaux, and J. V. Ringwood, "A nonlinear extension for linear boundary element methods in wave energy device modelling," *Proc. 31st International Conference on Ocean, Offshore and Arctic Engineering. American Society of Mechanical Engineers*, vol. 4, p. 615–621, 2012.

[6] W. E. Cummins, "The impulse response function and ship motions," Tech. Rep., 1962. [Online]. Available: http://hdl.handle.net/1721.3/49049

[7] S. Y. Kung, "A new identification and model reduction algorithm via singular value decomposition," *Proc. 12th Asilomar Conf. on Circuits, Systems and Computers, Pacific Grove, CA, November, 1978*, 1978. [Online]. Available: https://ci.nii.ac.jp/naid/10024448775/en/

[8] G. G, M. Penalba, and J. Ringwood, "Nonlinear hydrodynamic models for heaving buoy wave energy converters," in *Proc. Asian Wave and Tidal Energy Conf.*, 2016.

[9] L. E. Borgman, "Random hydrodynamic forces on objects," *Ann. Math. Statist.*, vol. 38, no. 1, pp. 37–51, 02 1967. [Online]. Available: https://doi.org/10.1214/aoms/1177699057

[10] J. Falnes, *Ocean Waves and Oscillating Systems: Linear Interactions Including Wave-Energy Extraction*. Cambridge University Press, 2002.

[11] A. Babarit and G. Delhommeau, "Theoretical and numerical aspects of the open source BEM solver NEMOH," in *11th European Wave and Tidal Energy Conference (EWTEC2015)*, ser. Proceedings of the 11th European Wave and Tidal Energy Conference, Nantes, France, Sep. 2015. [Online]. Available: https://hal.archives-ouvertes.fr/hal-01198800

[12] D. N. Veritas, "Dnvgl-rp-c205 environmental conditions and environmental loads," Tech. Rep., 2017.